Competitive Chloride Chemisorption Disrupts Hydrogen Bonding Networks: DFT, Crystallography, Thermodynamics, and Morphological Consequences

Laurence Marks[‡]

ABSTRACT

The consequence for aqueous corrosion of chloride ions in an aqueous environment on the surface structure and thermodynamics of hydroxylated magnesia (001) and alpha-alumina (001) and (100) is analyzed using density functional methods. It is shown that there is competitive chemisorption between hydroxide and chloride, with the chloride disrupting the hydrogen bonding network on the surface. There is a significant crystallographic dependence, as well as dependencies upon the environment in terms of the pH and chloride molarity. An analysis of the results in terms of existing, competing models in the literature for the effect of chloride indicates that rather than the existing models being competitors, most are correct but incomplete. Rather than the different models being viewed as competitors, or each being rate determining for some specific set of conditions, the majority are simultaneously correct. Conventional oxide surface science extrapolation of the results yields qualitative conclusions for the effects of, for instance, alloy dopants which are consistent with existing experimental data. The analysis also indicates the existence of a number of new phenomena in corrosion, for instance local galvanic couples due to the work-function change with chloride chemisorption, as well as thermodynamic dewetting of the oxide film.

KEY WORDS: adsorption, chloride, density functional theory, surface structure

INTRODUCTION

It is well established that many engineering metals form protective oxide coatings in air or aqueous conditions, without which they would be unusable. The science of how these coatings form, what oxides are present, and how the protective layer changes as a function of time is an issue of prime importance to control or mitigate corrosion, both general corrosion as well as pitting or crevice corrosion. While water by itself is an aggressive environment for many materials, the addition of chloride ions frequently can lead to substantially faster corrosion, in some cases the protective oxide film develops pits, pinholes, or can otherwise fail so the bare metal is attacked. This is important not just for applications where there is exposure to seawater which has approximately 0.6 molar salt, but also biological applications where there are concentrations of about 0.1 molar salt in the vicinity of metal devices used in implants. One does not want the expense of continually applying coatings or just paint to metals to protect them during use, and this is obviously problematic for implant devices within patients.

There have been decades of research at the more macroscopic level to understand how chloride increases corrosion. It is now well established that it can lead to inhomogeneous local breakdown processes. For instance, small pits (pinholes) develop in the oxide film which can then grow with attack of the underlying metal, progressively undercutting the oxide until they become large enough to be observed with optical microscopes or sometimes by direct visual inspection.

CORROSION—Vol. 74, No. 3

295

There is significant empirical understanding of how to reduce this effect, for instance by the addition of molybdenum or other alloying elements (e.g., references[1-9]). What is taking place at the atomic scale both with and without these additives, as well as full details of how breakdown occurs is not as yet fully understood. Many different models exist, as will be discussed further in the next section, but there is little general consensus and often the models are considered to be conflicting, i.e., one is right and the other(s) wrong.

The focus of this report is a closer analysis at the atomic scale of the processes taking place when chloride ions are added to protective oxide coatings in an aqueous environment. This is examined using density functional theory (DFT) methods to understand what matters, what does not in terms of how chloride ions change the surface structure and thermodynamics. What will be shown is that the problem involves competitive chemisorption between surface hydroxide and chloride, with the chloride disrupting the hydrogen bonding network at the surface. The main effect of chloride is to significantly reduce the surface free energy of the surface, which can lead to morphological instabilities. From an analysis of the thermodynamics for different crystallographies it appears that most of the apparently conflicting models are simultaneously correct, albeit each by itself only considers part of the overall processes occurring. The analysis also reveals one unexpected effect, namely that chloride chemisorption increases the oxide work function which can increase the oxidation rate (as explained later).

The structure of this report is as follows. The next section provides some general background to the existing model and closely related numerical literature, primarily so later the connections can be made to the results of the density functional calculations. To make this clearer, some general concepts of Driver, Trigger, Mechanism, and Dependencies are introduced, to differentiate between whether specific models are describing how the thermodynamics is changing or, for instance, the atomistic processes. This connection will be returned to later in the discussion. After this background section, the numerical DFT methods will be briefly described followed by the structural results and energetics. While these results are comparable to the prior literature (cited later), there are some significant additional details that will be described. This is followed by an analysis of the thermodynamics where the molarity of the chloride ion as well as the pH is included. Finally, the results are placed within the general context of aqueous corrosion, showing that many of the previous models for the role of chloride are simultaneously correct, albeit each by itself is an incomplete description. Conventional oxide surface science extrapolation of the results yields qualitative conclusions for the effects of, for instance, alloy dopants which are consistent with existing experimental data.

BACKGROUND

The literature on the effect of chloride is a complicated and controversial; for some general reviews see references.[10-17] The majority involves some experimental evidence, and based upon this models have been qualitatively proposed, often not fully detailed. There are also a few cases where aspects of the thermodynamics have been calculated using DFT methods, although these have some gaps. Much of the literature is a proponent of one particular model, by implication the other models being wrong. As will become clearer later, the analysis herein indicates that most of the models are correct, but they only describe part of a combination of thermodynamic effects.

Before providing a brief overview of the literature where models are developed or analyzed, it is important to introduce a number of terms to facilitate description of what the different models currently available describe. This involves differentiating between what will be called *Drivers*, *Triggers*, *Mechanisms*, and *Dependencies*.

A *Driver* is the relevant free energy term that controls the thermodynamics. By definition, a Driver must correspond to a reduction in the free energy of the system, either in a closed thermodynamics sense or open thermodynamics, where the total system is considered including the environment.

A *Trigger* is the local process which subsequently leads to a change such as breakdown of the protective oxide film. This is associated with some local morphological change, often a morphological instability that leads to a runaway process such as breakdown.

The *Mechanism* is the atomistic or nanoscale process that leads to the change. It frequently is associated with a specific structural Trigger, and has to be in response to some Driver.

The *Dependencies* are how all of the above depend upon the external environment, for instance the pH, temperature, and applied potentials.

It is also relevant to expand slightly on the concept of a morphological instability (e.g., references[18-34]), as this will be central to much of the analysis of the results herein, although details will not be provided. In most cases we are dealing with a change from a conformal oxide protective coating to a discontinuous film. The discontinuous film has a larger surface area, so the surface free energy of the oxide is a stabilizing Driver that will oppose the formation of a discontinuous film—the energy cost of the new surfaces. Of necessity, there has to be some other destabilizing Driver, for instance a net gain in elastic energy due to the relief of stresses in the oxide. In morphological instability theory, one describes how the system behaves with respect to perturbations of a finite

wavelength. If these lead to a net free energy reduction, the perturbations will grow and can accelerate with time, leading to a breakdown event—typically observed as a spike in the electrochemical response (electrochemical noise). From an analysis of the free energy, change parameters such as the growth rate, size scales, and incubation times can be estimated.

For completeness, some of these concepts are implicit in the early work such as that of Hoar[35] who suggested that chloride chemisorption would reduce the stabilizing surface energy driver, Sato[36] who considered electrostriction as the destabilizing Driver and surface energy as the stabilizing Driver, and also Xu, et al.,[37] who considered pitting via a balance of field-induced stresses and surface energy. More recently, Tang and Ballarini[38] have analyzed numerical details of the morphological instability problem for electrostriction and Heuer, et al.,[39] also included flexoelectric[40] contributions.

Turning now to the existing literature, one of the earliest models is the Adsorption/Aggressive Ion model.[41-45] In this model, there is a local accumulation of chloride that leads to local thinning, then breakdown. The details of why in some regions chloride chemisorption occurs and not others has not been well explained to date. Considerable work is present in the literature on the chloride Dependencies, less on the atomistic and energy details.

A second approach, related to the first is that chloride is somehow incorporated subsurface and/or at grain boundaries and leads to increased stresses, e.g., references.[35,37,43,46-50] The destabilizing Driver would then be release of the strain energy, but the Driver for why the chloride becomes trapped subsurface or at grain boundaries is not clear, and the Trigger is not well defined. While chloride incorporation into a hydroxide is reasonable, the chloride ion is too large to be incorporated into a close-packed oxide as a substitutional point defect, as verified by DFT calculations.[51-53]

A third approach is that surface chloride increases the concentration and mobility of metal vacancies.[14,54-56] As a consequence of metal vacancy, diffusion voids can form at the metal/oxide interface with subsequent thinning of the oxide film or fracture. As structured this is a Mechanism, with the Kirkendall voids[57-63] the Trigger, but the Driver(s) are not specified.

In some models the chloride is in some fashion connected to morphological instabilities and electromechanical stresses such as electrostriction—the relief of this free energy term would be the destabilizing Driver as mentioned above. As mentioned earlier in the work of Hoar[35] and Sato,[36] it was recognized that chloride could be reducing the stabilizing Driver of the surface free energy. However, the details have not been extensively followed up on, although as will become clear later this is a very significant factor.

A final approach is that chloride can lead to aqueous MCl_x complexes such as the tetrachloroaluminate ion (e.g., references[64-65]) which (open system thermodynamics) will increase the dissolution rate of the oxide by reducing the free energy of the metal in solution and hence lead to instabilities (e.g., Traubenberg and Foley[66]). Why this should lead to local breakdown is not clearly defined, and this is more an analysis of Dependencies, not the Driver.

Overviewing these different models, many as well as other literature analyze Dependencies, some deal with the Mechanism, most do not specify the Driver in detail, and none appear to explain why there should be local changes rather than conformal changes in the oxide. It is also not clear how the overall environment (Dependency) is important; this is not connected in detail. The true physical problem has to have Drivers, Triggers, and Mechanisms (there may be more than one) which make scientific sense and are consistent with established thermodynamics and structural concepts.

In terms of numerical calculations, there is a very large body of work for chemisorption onto metals particularly in the catalytic literature which are relevant for the initial monolayer stages of corrosion, but much less on chemisorption onto oxides. For the specific systems here (rocksalt and corundum structures), a number of calculations have considered by ab initio methods the base hydroxylated oxide structures, e.g., references,[67-83] both dissociated and molecular adsorption of water, others the additional effects of chloride.[15,51,77,84-87] In many respects these papers are at the opposite end compared to the others, as they do not involve so much the Mechanism, Dependencies, and Triggers. Instead they discuss the Driver/thermodynamics for specific crystallographies. In aqueous conditions the chemical potential of the water in the environment is high enough that every exposed oxygen has a hydrogen attached, every metal a hydroxide, within the constraints of valence neutrality, i.e., the metal is in the established valence state not anomalously oxidized or reduced. Oxidation, nonstoichiometric oxides and point defects are beyond the scope of this report. For the hydroxylated surfaces of corundum structure materials (e.g., Cr_2O_3 or Al_2O_3) it is established that hydrogen bonding is important (e.g., references[67-68,70,78-79,82]), a point that will be returned to; for rocksalt structure (e.g., MgO or NiO) there is no evidence that hydrogen bonding plays a significant role in the hydroxylated structures (e.g., references[73,75]).

In the presence of chloride, some papers have analyzed slightly different chemistries such as the adsorption of small molecules[15,67-68,70,77,84-88] on oxide surfaces, which is a different chemical problem. There has been less analysis on the specific problem of importance, the interaction of chloride with the hydroxylated surface.[15,51-53,89-90] All of these have been targeting the Driver associated with chloride, but

have only been for the rocksalt structure, which does not have hydrogen bonding. While these papers have provided important information, they have only considered relatively high surface concentrations of chloride (which may be physically unreasonable) and have not fully explored the thermodynamics as a function of the Dependencies of pH and chloride molarity. As will be seen later, some of the results herein are comparable as MgO is comparable to NiO, but beyond the (111) surface the results are quite different.

NUMERICAL METHODS

The alloys in most common use produce the oxides NiO, Cr_2O_3, and/or Al_2O_3. While NiO can be calculated using more advanced DFT methods, the available evidence indicates that the hydroxylated structures of MgO and NiO are very similar.[73,75] MgO can be calculated much more accurately using density functional methods than NiO so will be used herein as a model. Chromia is slightly more complex than alpha alumina due to the antiferromagnetic ordering, and is harder to calculate to a high degree of accuracy so only Al_2O_3 will be considered herein (hereafter the "alpha" will be omitted). Work is in progress for NiO and Cr_2O_3 using GGA+U methods and will be published elsewhere at a later date; semi-quantitatively the results are the same, the key differences being changes in the exact numbers.

DFT calculations were performed with the all-electron augmented plane wave + local orbitals WIEN2K code[91] using the PBE[92] functional. In all cases, inversion symmetry surface slabs were used with a fixed number of cells and vacuum size normal to the surface, and valence neutral structures so as to avoid artifacts with charged cells or highly reduced or oxidized compositions. Lattice parameters were those for the DFT relaxed bulk structures. For the calculations, muffin-tin radii of 1.85, 1.6, 1.6, 1.2, and 0.55 au were used for the Cl, Mg, Al, O, and H atoms, respectively; the plane wave extension (RKMAX) value was 2.5, equivalent to 281 eV, using Fourier coefficients for the potential (GMAX) to 20 au; and the Brillouin-Zone sampling was approximately one point every 0.5 nm^{-1}, reduced to either a single special point or the gamma point for the largest cells. To ensure reasonable convergence for cross-validation (see below) using a higher level functional, the exchange-correlation potential was calculated using an over-sampling of 1.8 for the plane waves and a quadrature of the spherical harmonics up to $L = 18$, using a Kahan summation[93] to improve numerical accuracy. All surface slabs had inversion symmetry, with the cell size normal to the surface approximately 4 nm, with 2/3 of the cell occupied by atoms so the region of vacuum was approximately 1.3 nm. This corresponds to 21 atoms for the smallest calculation and 616 for

the largest; chloride coverages ranged from a full monolayer to 1/18 of a monolayer. A few additional structures were calculated which had significantly higher enthalpies, and are not described further. All atom positions except those fixed by symmetry were relaxed to an accuracy of 1 mRyd/au or better using a parallel quasi-Newton algorithm.[94] Some care was needed to ensure that the atom positions were properly minimized when there was hydrogen bonding, as these lead to soft modes and also rotations of bonds. There was still a little "noise" in the calculated energies of ~1 meV (which will be shown later in the figures) due to numerics and intrinsic differences in the configuration of the chloride for the larger cells, although this was well below the absolute accuracy of the DFT energies due to limitations of the functional; convergence accuracy and the absolute accuracy of DFT calculations are not the same.

For strongly ionic solids such as MgO and Al_2O_3, the PBE GGA represents the ionicity quite well. As a cross-validation, additional calculations were performed using the SCAN metaGGA functional[95] with the published fit for the additional dispersion corrections[96] using a recent non-local approach.[97] The differences are exceedingly small, as would be expected from prior experimental and theoretical work for MgO and NiO surfaces.[73,75]

The chemistry of the valence neutral surfaces of these oxides is well established (see references in the previous section), so there was no need to establish the basics. For the MgO (111) surface, the hydroxylated 1×1 surface was used as the starting point, and the similar fully hydroxylated surfaces were used for Al_2O_3 (001) and (100). The conventional three-index hexagonal notation will be used for Al_2O_3. From the conventional chemistry of valence neutral oxide surfaces (e.g., Enterkin, et al.,[98] and references therein), chloride will replace OH groups on these surfaces; note that there is now extensive evidence that similar to bulk oxides, oxide surfaces obey the fundamentals of inorganic chemistry such as Pauling's rules.[99] The size of the repeat unit in the surface was changed to obtain a wide range of surface compositions, keeping all other parameters of the calculations constant to avoid artifacts.

For the thermodynamic calculations, calibrants for the bulk energy of MgO and Al_2O_3 were used with matching RMTs and RKMAX. For water an isolated H_2O molecule was calculated in a $10.9 \times 12.9 \times 12.9$ au right-angle cell, and the experimental free energy of condensation used to obtain the reference for liquid water at standard temperature and pressure. For the chloride bulk references of NaCl and NaOH were used and the experimental free energy of dissolution in water. All thermodynamic quantities were then calculated using conventional ab initio thermodynamics, omitting the smaller entropy contributions (see later).

No density functional calculation is perfect, and unless care is taken it is possible to obtain misleading results; some additional discussion is provided in the *Appendix*. The use of the PBE function is a reasonable approximation because it yields quite good heats of formation for oxides such as those here, albeit not so good for surface enthalpies. Because the size of the slabs normal to the surface was kept constant, most systematic errors should cancel when structures are compared, the largest errors being in absolute terms such as the surface free energies which might have an offset compared to experiment. As will become apparent later, while the numerics provide insight into the Drivers that matter, in a true engineering system the oxide will be highly inhomogeneous so the exact numbers herein cannot be directly applied, although one could produce empirical models where the right functional dependence is included in the future.

For completeness, the only assumptions in the calculations are:

(i) The functional, which is based upon the existing literature as well as prior work which included error analysis and obtained reasonable agreement between experiment and theory for comparable ionic hydroxide surfaces.[73,75]

(ii) The neglect of entropy, although this is mentioned in several places particularly configurational entropy.

(iii) Analytic continuation in the thermodynamics.

(iv) Convergence criteria and other numerics, which are reasonable for large calculations.

NUMERICAL RESULTS

In this section, the main theoretical structural and energetic results will be described, broken down into subsections for MgO (111), Al_2O_3 (001), and Al_2O_3 (100). In the *Thermodynamic Analysis* section, the thermodynamics will be analyzed where these are combined with the chemical potentials to examine the effect of the environment on the surface energy Driver, with general discussion of the implications in the *Discussion*.

MgO (111) Surface and Some General Results

The results for MgO (111) are comparable to previous work for NiO (111).[15,51-53,89] The key result for the MgO (111) surface is that it is quite simple. Along [111] the structure contains alternating close packed hexagonal planes of Mg and O atoms. At the surface, the base hydroxylated structure has tetrahedral O atoms, each bonded to three Mg below with the hydrogen vertical as shown in Figure 1. In this geometry there is essentially no hydrogen bonding within the surface. In principle the hydrogen atoms would be in an energetically lower configuration if they could rotate into the plane of the surface so they could hydrogen bond to adjacent oxygen atoms. However, this would

place them close to the Mg^{2+} ions and the associated Coulomb repulsion of the cations is energetically prohibitive, so this does not happen. The full atomic positions are available as a crystallographic information file (CIF) in the supplemental material.

Chloride chemisorption replaces the OH^-, competitive chemisorption, as previously discussed in the literature (e.g., Marcus, et al.[50]), with the chloride sitting quite high (close to the location of the hydrogens) because it is a significantly larger ion. This is a simple Ising-type problem on a hexagonal lattice, with each position occupied by OH^- or Cl^-. For the naturally hexagonal rocksalt (111) surface, the corundum (001) as well as the more complex corundum (100), the chloride arrangement is lowest in energy when they form a two-dimensional hexagonal supercell—which is the arrangement that yields the largest chloride-chloride distances for a given coverage. As a function of the surface composition of chloride there is minimal change in the local geometry, see Figure 1, except for the metal-chloride bonding; full details for the different structures are available as CIFs in the supplemental material.

A useful parameterization is the bond-valence sum (BVS) of the chloride, which is exponentially related to the bond-length. For surfaces this provides a good metric of the local bonding.[98] If the values are close to the nominal valence, this indicates a favorable bonding for the particular site. For surfaces values are typically 10% to 20% lower than the bulk. There are two contributions to the bonding of the chloride, a local stronger bond to aluminum (local-BVS below) and a weaker long-range dipole interaction with the hydroxides, and values for both the total BVS and only that for the Al-Cl bond (local-BVS) are discussed below and shown in Figure 2. At low coverages, the Al-Cl bond-distance is significantly larger and the local-BVS is 0.5 to 0.7 of what it is in the bulk chlorides, the rest being the weaker dipole term. The local-BVS increases approximately linearly with coverage with the chloride over-bonded for high coverages. For the higher coverages the chlorides are close enough that there nominally could be some covalent bonding between them; the local-BVS shown do not include these contributions. This is general for all of the surfaces herein although the slopes differ and the changes for the Al_2O_3 (100) surface are weaker; the data are collated in Figure 2, scaled to the BVS of the corresponding bulk chlorides. As will be seen in the *Thermodynamic Analysis* section, the very high coverages are not physically meaningful as the surface is unstable under conditions where they would occur or would involve unreasonably high chloride concentrations in solution.

A second generalization for this and the other surfaces is that chloride substitution for hydroxide leads to a significant increase in the work function of the oxide, see for instance Figure 3, which has consequences for oxidation rates as discussed later. For
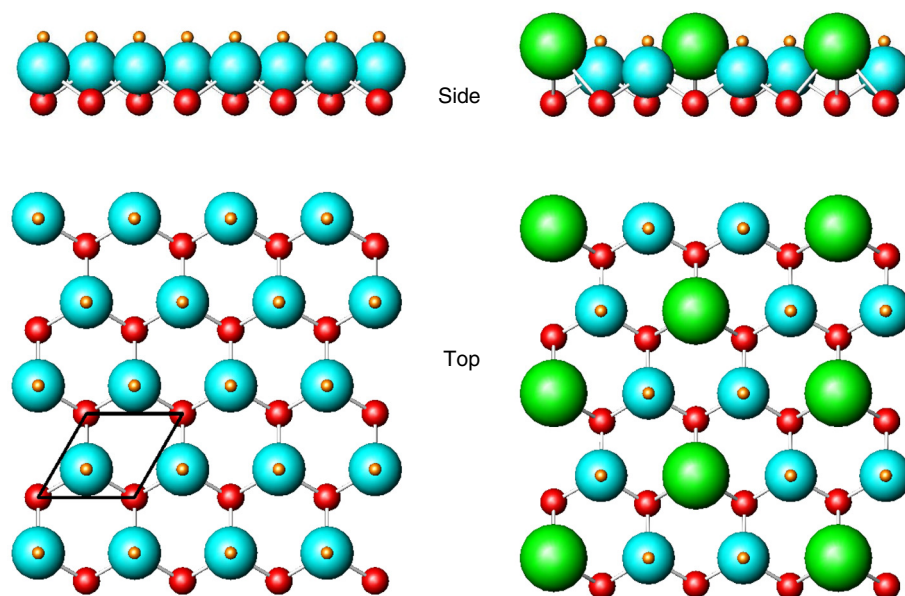
FIGURE 1. *Structures on the MgO (111) surface. On the left, the 1 × 1 hydroxylated surface viewed from the side and on top, with the surface unit cell indicated. On the right, the chloride surface where one-third of the hydroxides have been replaced by chloride. The metal atoms are red, oxygen are blue, hydrogen are orange, and chlorine are green. Only the surface of the structure is shown; full atom positions are available in the supplemental material.*

completeness, note that the work function, i.e., the difference in energy between vacuum and the highest occupied state is a ground state property, so is in principle fairly accurately calculated with conventional DFT. The work function increases with coverage, saturating at about one-third of a monolayer. For completeness, the full coverage case for Al_2O_3 (001) is not shown, as the work function is anomalously low at 4.7 eV. The source of this is the difference in the
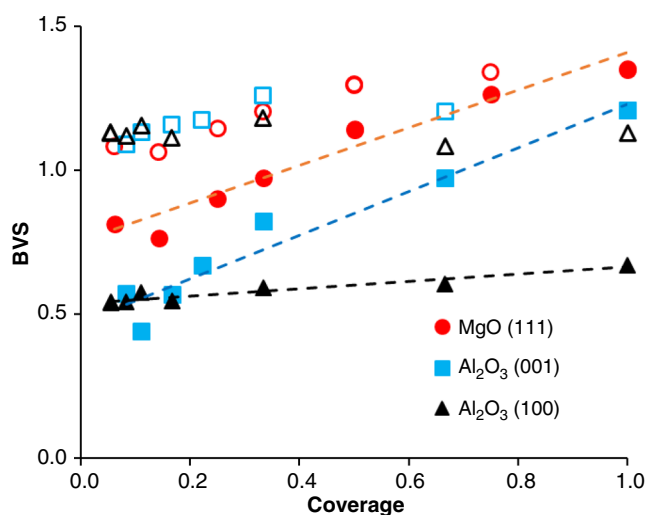
surface dipole for metal-hydroxide bonding compared to metal-chloride. The values for the difference will change in solution, being partially compensated by changes in the double-layer outside the surface, but the trend should not change. Isolating charge transfer for extended basis set method (as against orbital basis sets) is not simple; one approach is to use the Bader charges[100] which gives a measure of the total electron density for each atom. The difference between the valence and the Bader charge is interpretable as the ionicity and linked to but different from the "charge" of an atom, which is not well defined in DFT. The electrochemical charge is the valence. The Bader charges for the hydroxyl group and the chloride are
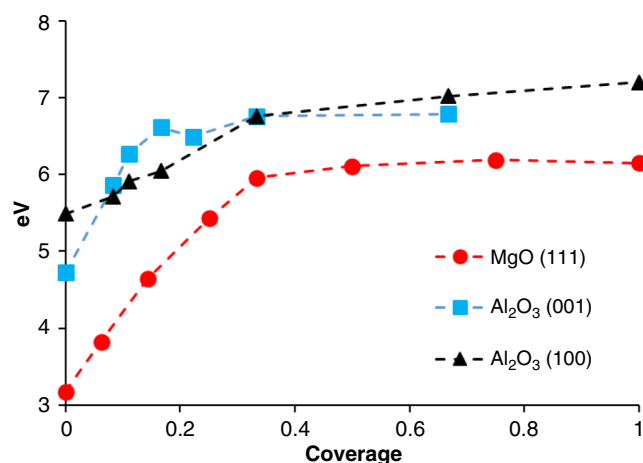

FIGURE 2. *Bond valence sum (BVS) of the chloride versus coverage, normalized to that of the chlorine in $MgCl_2$ and Al_2O_3. Solid markers are for the local Al-Cl contribution only, and hollow markers are for the full BVS including the OH–Cl interaction.*

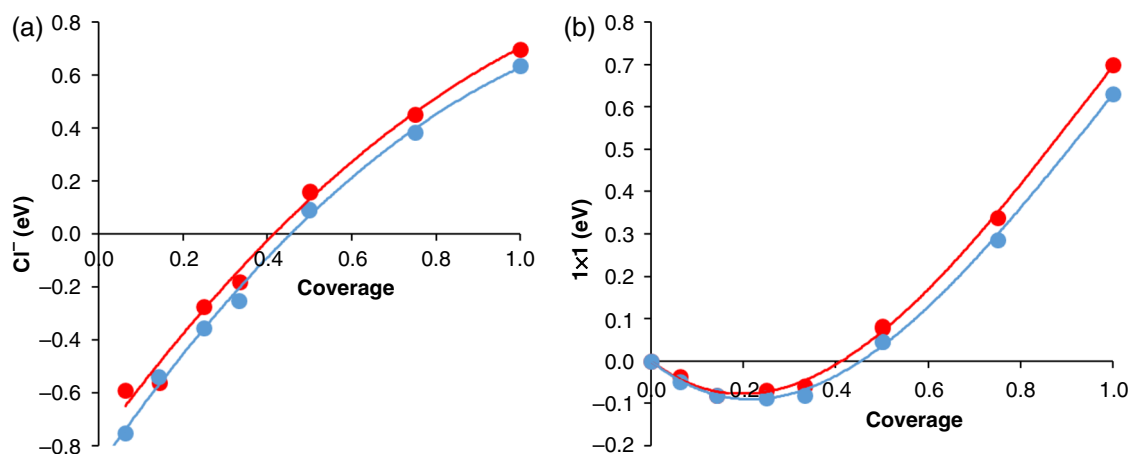**FIGURE 3.** *Variation of the work function with chloride coverage.*

FIGURE 4. *Enthalpy of the MgO (111)-Cl surface with coverage: (a) per chloride, and (b) per 1 × 1 surface unit cell. In both cases results for the PBE GGA are shown in blue, and the SCAN functional with a dispersion correction are shown in red.*

within 4% of the corresponding bulk chloride/hydroxide reference values and do not change significantly with coverage, approximately –0.85 for the Mg compounds and –0.8 for alumina. Hence, there is minimal change in the ionicity relative to corresponding bulk compounds. The difference between hydroxide and chloride is due to the dipole of the hydroxide, the oxygen has a Bader charge of –1.42 and hydrogen 0.56 for the MgO (111) surfaces; the negative end of the hydroxide dipole points into the bulk oxide. As a caveat, the functional used here is known to overestimate the covalency, so the true iconicity will be slightly higher than the above numbers.

The enthalpy of the surface (uncorrected for the important chemical potential terms for the environment, for which see the *Thermodynamic Analysis* section, where the full ab initio thermodynamics is performed[101-102]) as a function of the surface coverage of chloride, as well as per chloride is shown in Figures 4(a) and (b) using both the GGA and meta-GGA methods, and is relatively simple. Here the saturation coverage is defined as unity, and Figure 4(b) is equivalent to Figure 4(a) multiplied by the coverage. The free energy increases with coverage, which can be attributed to the strain within the chemisorbed layer and repulsive long-range Cl⁻ interactions, similar to previous work.[51] Note that this suggests a tensile surface stress tensor (the surface would like to expand) which can be a driver for a morphological instability.[103]

For completeness, substituting chloride for oxygen in the bulk structure was tested; this was energetically unfavorable. As mentioned earlier, the chloride ion is significantly larger than oxygen. Simple point substitutions break the valence neutrality and so will be energetically expensive as they require the creation of carriers (unless a hydrogen is lost). As mentioned earlier, replacing oxygen by chloride in the bulk is not chemically reasonable for a close-packed oxide.

Al_2O_3 (001) Surface

While the alumina (001) surface has some similarities to the rocksalt (111) surface, there are very significant differences. Along [001] there are again alternating hexagonal planes, but only two of the possible three metal sites are occupied. This changes everything because the bond between the oxygen and hydrogen at the outer surface can now rotate to lie above the space where there is a missing Al atom in the layer below, as shown in Figure 5. The surface 1 × 1 unit cell contains two alumina and three oxygen and is marked in Figure 5. As a consequence the lowest energy configuration as previously shown[67-68,70] has a third of the hydrogen atoms involved in hydrogen bonds to two-thirds of the surface oxygen with a bond distance of 2.07 Å (0.207 nm); the hydrogens that have rotated to exploit the intrinsic surface aluminum vacancy are hydrogen bonded to two oxygens. Tests were performed to analyze whether the relative orientation of the hydrogen bonding was a significant energy contributor, i.e., parallel across all unit cells or changing. It was not, although this means that one can have a rotational glass (e.g., Marks, et al.,[104] and references therein). By comparing calculations where the (001) surface is constrained to have P-3 symmetry and no hydrogen bonds, to the fully relaxed structure, the hydrogen bond to the two oxygens reduces the energy by 0.73 eV (17 kcal/mol), 0.365 eV per OH–H bond using the more accurate metaGGA, which is very significant. The hydrogen bonding also has a significant effect upon the work function, increasing it from 3.1 eV to 4.7 eV. This is consistent with the hydroxide dipole mentioned above, as a third of these are now in the surface plane rather than normal to it.

For completeness, in solution there will also be hydrogen bonding to water molecules in the liquid, and it is not impossible for the surface chloride to move further into the liquid, away from the oxide surface.
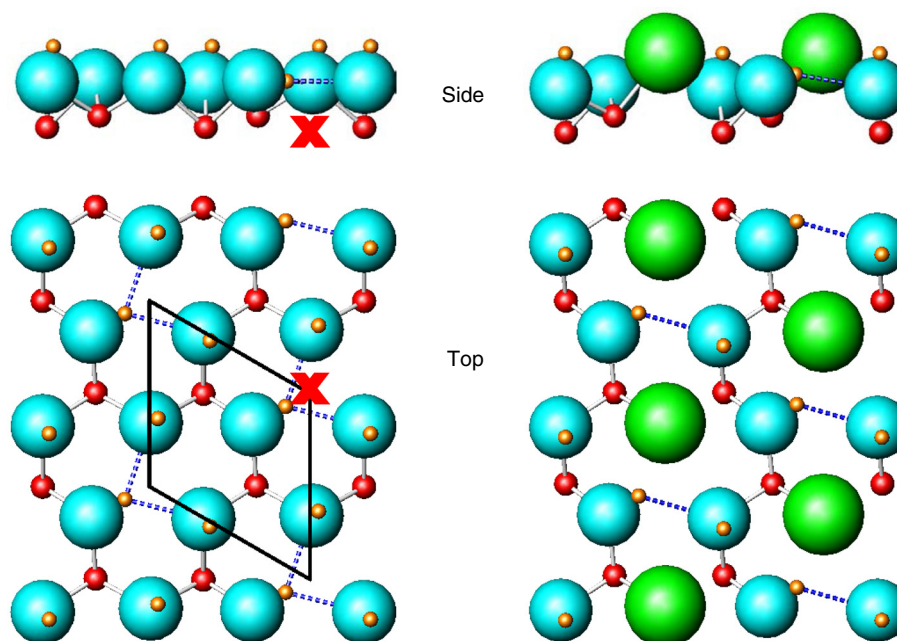
FIGURE 5. *Representative structures on the Al$_2$O$_3$ (001) surface. On the left, the 1 × 1 hydroxylated surface viewed from the side and on top, with the surface unit cell indicated. On the right, the one-third coverage chloride. The metal atoms are red, oxygen are blue, hydrogen are orange, and chlorine are green, and dashed lines in blue indicate the hydrogen bonding. As the unit of the surface, a projected unit which only contains one oxygen atom at the surface was used as the definition of the 1 × 1 surface unit cell and is marked on the left. The location of one of the intrinsic metal vacancies is marked with a red cross. Only the surface of the structure is shown; full atom positions are available in the supplemental material.*

Typical values for hydrogen bonds in water are about 0.1 eV[105] which means that they are not negligible. It will be interesting in the future to investigate DFT calculations with explicit water, although these calculations are likely to be prohibitively large for low chloride coverages.

Chloride replaces hydroxide, but also disrupts the hydrogen bonding network as shown in Figure 5. To estimate the non-local contribution of the OH–Cl bonding, a calculation was performed starting from the P-3 structure without hydrogen bonding with a single hydroxide replaced by chloride, and only the positions normal to the surface of all of the other atoms were allowed to vary. Combining this with the other numbers and a standard Born-Haber cycle, the OH–Cl interaction was estimated to be ~0.05 eV, significantly smaller. To give numbers that are comparable to other relevant surfaces, a surface area unit will be used that would be the area for a full monolayer coverage, i.e., three chlorides in the surface 1 × 1 cell, which will be referred to as the monolayer area. The raw energetics show a much weaker chemisorption enthalpy, as shown in Figure 6 for both the GGA and metaGGA methods; the values per chloride atom are almost perfectly linear with the coverages. Similar to the earlier case, this is largely a strain energy term. Full details for the different structures are available as CIFs in the supplemental material.

Al$_2$O$_3$ (100) Surface

This surface is different from MgO (111) and Al$_2$O$_3$ (001) because it does not have a simple layering order; instead six oxygens in the outermost layer and six in a plane with the aluminum are hydroxylated forming a hydrogen-bonding network (similar to previous literature[78-79,82]) as shown in Figure 7. Only single hydrogen bonds with lengths between 1.65 Å (0.165 nm) and 2.0 Å (0.20 nm) are present. As the unit of the surface (for the *Thermodynamic Analysis* section), a projected unit which only contains one oxygen atom at the surface was used, which is one-sixth of the surface 1 × 1 cell. As shown in Figure 7, the replacement of hydroxide by chloride disrupts this hydrogen bonding network, but less than for Al$_2$O$_3$ (001). As a consequence the raw enthalpies (Figure 8) for both the GGA and metaGGA methods are intermediate between the two cases. Full details for the different structures are available as CIFs in the supplemental material.

For completeness, this surface could accommodate a double-layer of chloride. However, in order to maintain the in-plane lattice of the underlying oxide the chlorides will be far too close, and the energy per chloride will be prohibitively large. On full minimization of the atomic positions, the double-layer chloride coverage spontaneously decomposed into a single-layer chloride coverage and two AlCl$_3$ molecules in the vacuum per surface unit cell. For completeness, we
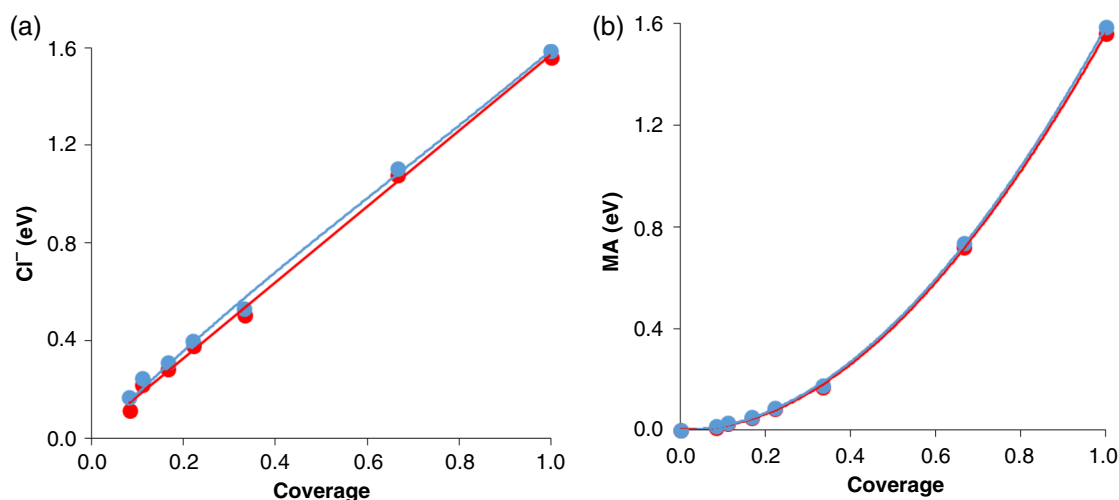
FIGURE 6. *Enthalpy of the Al$_2$O$_3$ (001)-Cl surface with coverage: (a) per chloride, and (b) per monolayer area (MA), which is one-third of the surface 1 × 1 unit cell. In both cases results for the PBE GGA are shown in blue, and the SCAN functional with a dispersion correction are shown in red.*
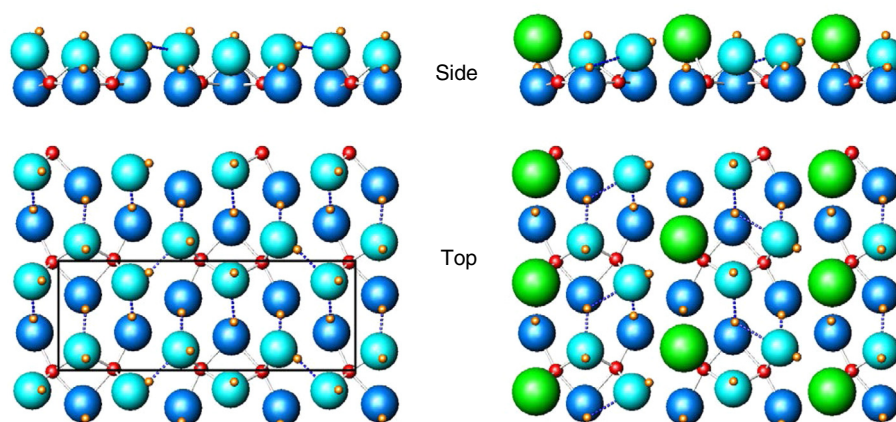

FIGURE 7. *Representative structures on the Al$_2$O$_3$ (100) surface. On the left, the 1 × 1 hydroxylated surface viewed from the side and on top, with the surface unit cell indicated. On the right, the one-third coverage with chloride. The metal atoms are red, oxygen are blue, hydrogen are orange, and chlorine are green, and dashed lines in blue indicate the hydrogen bonding. For clarity, a darker blue is used for the second-layer oxygen atoms. As the unit of the surface, a projected unit which only contains one oxygen atom at the surface was used as the definition of the 1 × 1 surface unit cell and is marked on the left. Only the surface of the structure is shown; full atom positions are available in the* supplemental material.

compared this structure and also the corresponding form where the Cl⁻ was replaced by OH⁻ with the monolayer coverage based upon the fully hydroxylated structure of Figure 7, and they were significantly higher in energy so would not occur and will not be described further.

THERMODYNAMIC ANALYSIS

From the previous section, it is apparent that chloride chemisorption competes with the hydrogen bonding network for the alumina-based surfaces due to the intrinsic metal vacancies just below the surface. For magnesia all metal sites are occupied so there is

no hydrogen bonding network (unless there are metal atom vacancies for other reasons).

The next step is to include the chemical potential of the chloride in solution as well as that of the hydroxide using conventional ab initio thermodynamics.[101-102] The relevant reactions are of a general type:

$$M-OH^- + Cl^- \rightarrow M-Cl^- + OH^- \qquad (1)$$
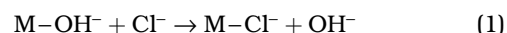
To convert to thermodynamic expressions, the free energy of this reaction per monolayer unit cell is given by:

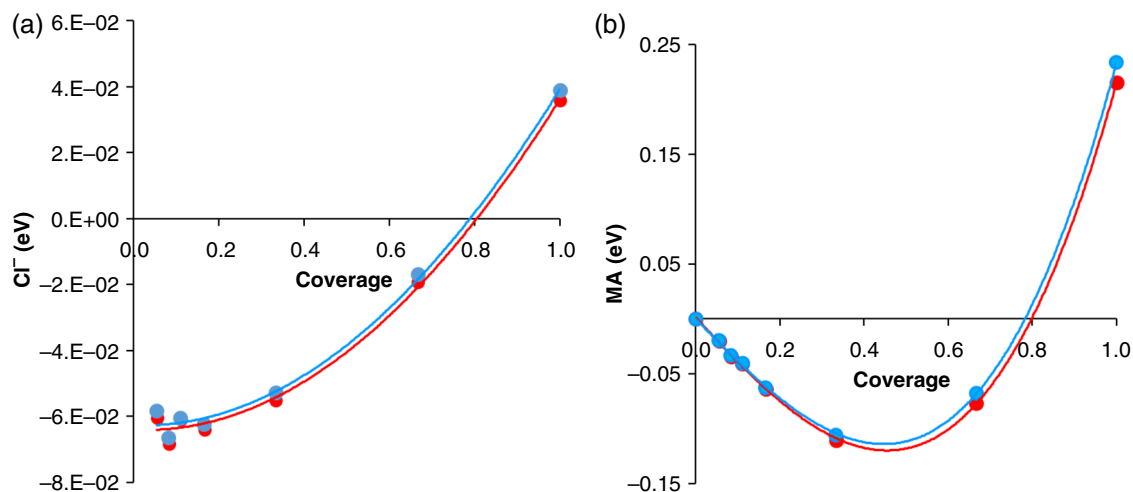$$\Delta G = G(M-Cl^-, f_{Cl}) - G(M-OH^-)$$
$$- f_{Cl}(\mu(Cl^-) - \mu(OH^-)) \qquad (2)$$

FIGURE 8. Enthalpy of the Al_2O_3 (100)-Cl surface with coverage: (a) per chloride, and (b) per monolayer area (MA), which is one-sixth of the surface 1 × 1 unit cell. In both cases results for the PBE GGA are shown in blue, and the SCAN functional with a dispersion correction are shown in red.
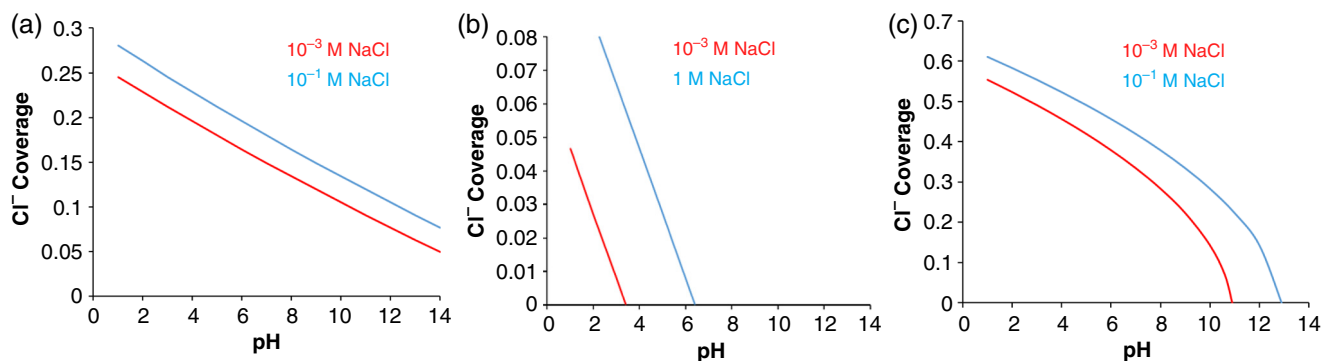

FIGURE 9. Chloride coverage as a function of pH and two different chloride molarities for (a) the MgO (111) surface, (b) the Al_2O_3 (001) surface, and (c) the Al_2O_3 (100) surface, using the dispersion corrected SCAN metaGGA.

where $G(M–Cl^-,f_{Cl})$ is the free energy per monolayer surface unit cell for the appropriate chloride coverage, $G(M–OH^-)$ is the corresponding hydroxylated surface free energy, and $\mu(Cl^-)$ and $\mu(OH^-)$ are the relevant chemical potentials of these species in water, which can be simply calculated from the pH and chloride ion concentration. At standard pressure and temperature the entropies of the surfaces will be small, so a reasonable approximation is to ignore these and use the enthalpies. There is a small configurational entropy for the chloride in a simple surface solution model which would be less than 0.015 eV/monolayer area, and can be reasonably neglected. To complete the analysis, the coverage will be when the total free energy is minimized as a function of surface chloride composition. To analyze this, the surface enthalpies for discrete coverages were extrapolated to smooth polynomials and the minimum energy coverage calculated analytically as a function of the chemical potentials.

This leads to a surface coverage that depends upon the crystallography of the surface, the molarity of the NaCl in solution, and the pH. Results are shown in Figure 9. Consistent with the discussion of the hydrogen bonding in the previous section, there is a high chloride concentration on the MgO (111) surface, a low concentration on the Al_2O_3 (001) surface, and a medium concentration on the Al_2O_3 (100) surface.

The final step in the analysis is to convert these numbers to surface free energies as a function of the pH and NaCl molarity as shown in Figure 10. The MgO (111) surface is only stable for relatively high pH values, and becomes unstable for low ones—i.e., spontaneous dissolution, as one would expect. In contrast the Al_2O_3 (001) surface has only a very small change in free energy and that for quite acidic conditions, the hydrogen bonded network is robust and resists the chloride. The Al_2O_3 (100) surface has a fairly high chloride coverage at low pH, and a significant reduction in the surface energy. The differences in the chemisorption and surface free energy as a function of material and the crystallography of the surface have significant impact, as will be discussed next.
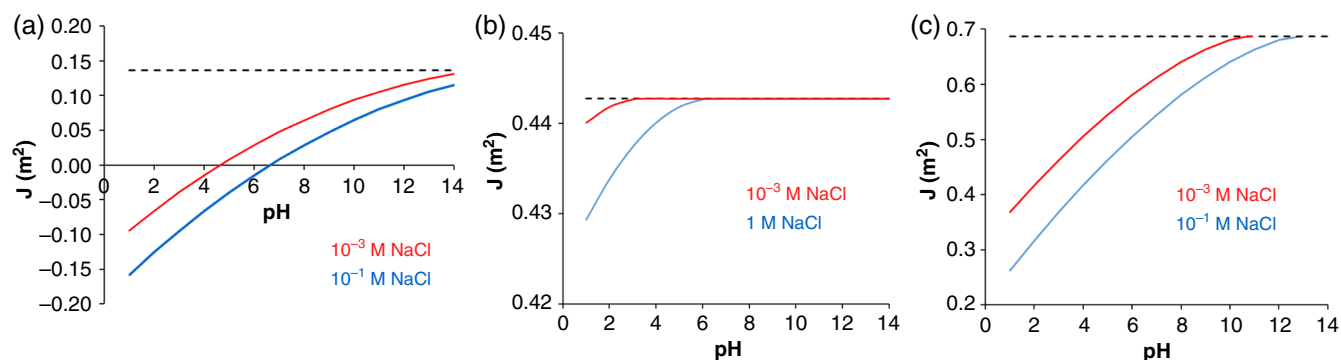
FIGURE 10. *Surface energy as a function of pH and two different chloride molarities for (a) the MgO (111) surface, (b) the Al₂O₃ (001) surface, and (c) the Al₂O₃ (100) surface, using the dispersion corrected SCAN metaGGA. In all cases the bulk surface free energy of the hydroxide in the absence of chloride is shown dashed.*

DISCUSSION

The focus of this paper has been to merge the existing, older results and models with extensive ab initio modeling of the role of chloride for a selected number of different surfaces. The analysis herein indicates that chloride in solution competes not simply with hydroxide, but also with the hydrogen bonded network on the oxide surface, with a crystallographic dependence and also a dependence upon the nature of the underlying metal geometry as the latter determines the hydrogen bonding possibilities. As mentioned earlier, work is in progress for NiO and Cr_2O_3 using GGA+U methods and will be published elsewhere at a later date; semi-quantitatively the results are the same, the key differences being changes in the exact numbers. This hydrogen bonding is not a small energy term; it is very significant and the DFT calculations indicate that it is about 0.73 eV (17 kcal/mol) per 1×1 unit cell for the Al_2O_3 (001) surface. This does raise a new general concept that the passivation of many metals in an aqueous environment has a significant contribution due to stabilization of the surface by comparable hydrogen bonding networks, which is disrupted by the addition of halides.

In terms of the concepts introduced earlier, the Mechanism is a crystallographic dependent competition between the hydroxide and the chloride. The relevant Driver that is changing is the stabilizing surface free energy as originally suggested by Hoar[35] and Sato.[36] At least in the analysis here the relevant Trigger is not defined; it will be one or more of those that are part of the existing models discussed in the *Background* section.

Turning to the models described in the *Background* section, several aspects are clearly backed by the DFT numbers:

1. The Adsorption/Aggressive Ion model is relevant; one has different chemisorption on different oxide faces. In addition, if instead of using an analytic extrapolation of the enthalpies one uses
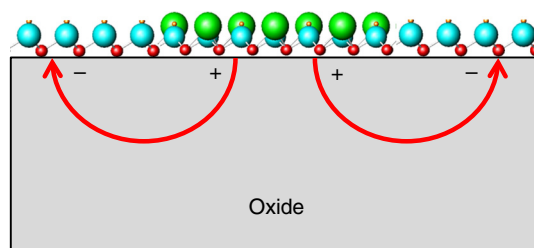

FIGURE 11. *Illustration of islands of higher chloride concentration (green) for a hydroxylated surface, with two of the electric fields lines due to the increase of the work function schematically illustrated in red.*

a more rigorous convex hull approach, the surface will have islands/domain structure which locally have a lower surface energy as illustrated in Figure 11. Due to the dependence of the work function on the chloride coverage, this will lead to local band bending and fields, which will lead to significant flexoelectric-induced stresses.

2. For models which involve chloride penetrating at grain boundaries, if these remain intact the analysis does not support this concept. However, there is a coupling of grain boundaries and surface free energy particularly at triple points. It is well established that there are grooves at grain boundaries which depend upon the surface free energy and the grain boundary energy. As a simple case, with an isotropic surface free energy in two dimensions one can construct a variant of a Wulff construction for a pair of oxide nanoparticles on an alloy substrate as shown in Figure 12(a) (see Marks and Peng[106] and references therein for background on this type of construction). In this case the metal will be exposed if $\sqrt{([\gamma_{GB}]^2 + 4\gamma_I^2)} < 2\gamma_S$, where γ_{GB} is the grain boundary free energy and γ_I the metal/oxide interface free energy. Extending this to a triple point as shown in Figure 12(b),
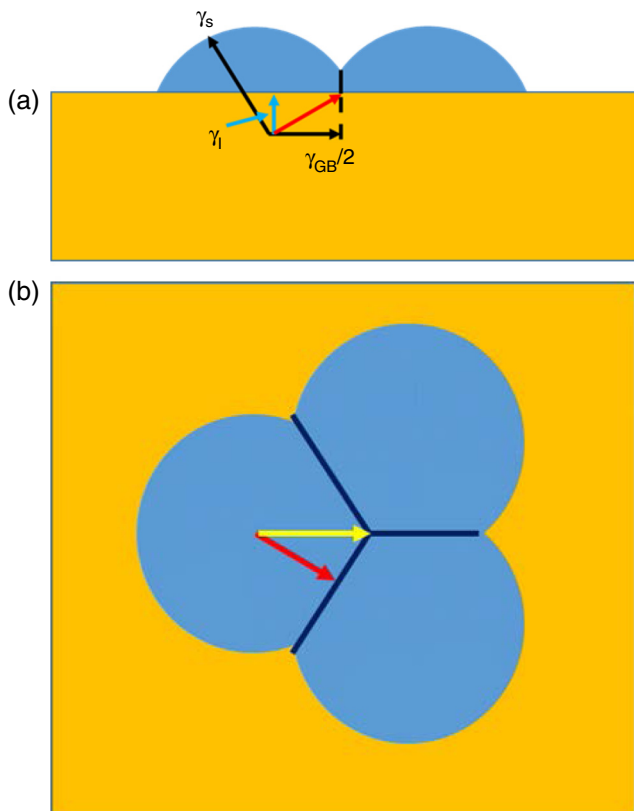
FIGURE 12. *Illustration of the effect of the surface free energy on apparent grain boundary etching, using a Wulff-construction approach. (a) The case for two oxide nanoparticles on a surface from the side, where γ_{GB} is the grain boundary free energy and γ_I is the metal/oxide interface free energy. The smaller the surface free energy, the larger the grooving at the boundary. (b) Top view of a triple-point, showing that in the thermodynamic lowest energy configuration metal can be exposed with a reduction in the surface free energy.*

thermodynamically the triple point will have bare metal if $\sqrt{(C[\gamma_{GB}]^2 + 4\gamma_I^2)} < 2\gamma$, with C = 3/4 for the isotropic case shown and in general will vary with the details of which facets are present in the Wulff construction under the relevant conditions. The Mechanism, removal of atoms at the grain boundary, is essentially the same as what exists in the literature, but the Driver is not the same.

3. In terms of models which involve stress relief with a Kirkendall void as the Trigger, or electromechanical stresses, chloride comes in directly as reducing the stabilizing surface energy Driver; stress relief is the destabilizing Driver.

4. Chloride chemisorption couples to surface metal vacancies, not through the concepts of point defect equilibria as previously discussed in the literature, rather more directly by breaking the hydrogen bonding network. Being specific, if there is a metal vacancy immediately below the

outer surface the hydrogens can rotate into the available space (similar to what occurs on the Al_2O_3 (001) surface) and stabilize the vacancy, increasing the energy barrier for it to move away. Replacing hydroxide by chloride removes this term, making the site available for occupancy by a metal atom. As mentioned above, the energy of the single hydrogen bond for the Al_2O_3 (001) surface is 0.73 eV (17 kcal/mol), which is not small.

The last point merits a little further discussion. Within the point-defect model, it was previously argued that chloride stabilizes metal vacancies via the reaction (using MgO as an example):

$$Mg_{Mg} + 2O_O + 2H_2O + 2Cl^-_{(aq)}$$
$$\rightarrow V''_{Mg} + 2Cl^{\cdot}_O + 4OH^-_{(aq)} + Mg^{2+}_{(aq)} \qquad (3)$$
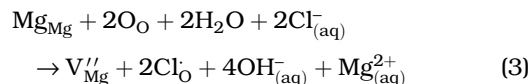
This is a reasonable reaction, with an appropriate Dependency upon both the chloride molarity and pH. It can occur for an open framework oxide where in the bulk there is enough space for the larger chloride ion to replace an oxide, but not in a close-packed oxide. It could occur in principle at an oxide surface where there is room for the chloride by relaxation of the atomic position away from the bulk, normal to the surface. However, it would be competing with the hydroxylation reaction at the surface, which can be written in an extended Kröger–Vink notation (ignoring charges) as:

$$Mg_{Mg,Surface} + O_{O,Surface} + H_2O(aq)$$
$$\rightarrow \{Mg_{Mg,Surface}OH_{Surface}\} + OH_{Surface} \qquad (4)$$
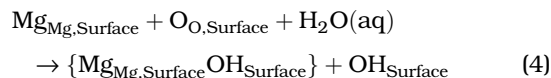
where the first term on the left is an exposed Mg at the surface, the second an exposed oxygen at the surface, while on the right the term in the brackets is a hydroxide chemisorbed onto the metal. It is plausible that some surfaces are present which do not readily hydroxylate, for instance the MgO (001) surface. However, in water these will be higher in free energy, so are thermodynamically less likely. There may be special cases, for instance cyclic treatments under dry and wet conditions where chloride could react with exposed oxide at a free surface, but in general this would appear to be unlikely.

An important conclusion is that in terms of the existing literature, it is not one model alone which is correct and all others are incorrect; rather the existing literature has pieces of the overall process and they are all somewhat correct, albeit incomplete. It should be stressed that the results support the view that rather than the different models being viewed as competitors, or each being rate determining for some specific set of conditions, the majority are simultaneously correct. There is no reason why multiple Mechanisms are not taking place in different regions, Triggered by different structure features, with common Drivers such as surface energy, stress, or electrostriction. There is

also an additional effect which does not appear to be in the current literature—the change in the work function. In terms of the original Cabrera-Mott model, [107] oxidation occurs via chemisorption of an oxidizing species which extracts an electron from the metal. This leads to band-bending across the oxide, and as the energy of the acceptor states in the oxidant at the surface become more positive, oxidation will be suppressed. The increase in the work function will offset this; hence chloride chemisorption can have the unexpected secondary effect of increasing the oxidation rate.

It may appear that the factor of two change in the surface energy for the Al_2O_3 (100) surface will not lead to large effects, but this is not the case. Using Dependencies from the literature, a morphological instability (e.g., references[18-34]) can be represented as a two-dimensional height change h(x, y, t) of form:

$$h(x,y,t) = h_0 \exp(\sigma(k)t) \exp(ikx) \tag{5}$$

where x is along the surface, y is normal to it, t is time, σ is the growth rate, and k is the wavevector of the instability. If $\sigma > 0$, the instability will grow exponentially. The general form of the growth rate is:

$$\sigma(k) = M(Ak^{n-1} - \gamma k^n) \tag{6}$$

where the order n depends upon the nature of the destabilizing Driver, M and A are constants, and γ is the surface free energy. For growth-dissolution, n = 2; for surface diffusion, n = 4; and for bulk diffusion, n = 3. This leads to a rate which is given by the maximum value of $\sigma(k)$ of:

$$\sigma_{max} \sim MA^n / \gamma^{n-1} \tag{7}$$

which also relates inversely to the incubation time. The order n as well as the exponential dependence will amplify the effect of even relatively small changes.

A few additional comments. DFT calculations can be very powerful to establish the thermodynamic framework for a particular class of problems. However, enough is now known about oxide surface chemistry that one does not have to perform a calculation for every problem. In particular, most of the rules[99] for valency, bond-order, and stereochemistry in inorganic chemistry and electrochemistry translate to oxide surfaces with minimal change. One can therefore make a number of semi-quantitative further conclusions:

(i) While the structures shown here are all ordered, these systems are Ising-type cases, as one would expect from an application of Pauling's rules.[99] Hence, there will be a configurational entropy similar to other cases for oxide surfaces (e.g., Marks, et al.,[104] and references therein). It seems unlikely at typical temperatures of aqueous exposure that these entropy contributions will be significant. However, one does expect a certain, perhaps large disorder due to kinetics, as the kinetics of changing from a disordered to ordered arrangement of chloride may well be slow.

(ii) The addition of higher valence metals, such as Mo, from valence neutrality conditions will increase the number of vacant sites in the metal layer just below the surface, facilitating hydrogen bonding and opposing chloride chemisorption. This correlates with known stabilizing contributions of elements such as Mo in Cr_2O_3 or in titanium alloys.

(iii) Lower valence dopants will in general increase the corrosive effect of chloride as the density of vacant sites in the subsurface metal layer will be smaller so hydrogen bonding will be weaker. This correlates with the effect of, for instance, Al in Ti alloys.

(iv) The size dependence of halide effects on corrosion are obvious because the heavier the halide, the larger it is and, hence, less able to fit into the confined space available when it replaces the smaller hydroxide ion, consistent with prior work (e.g., Bouzoubaa, et al.[53]).

(v) Fluoride is both smaller and has strong hydrogen bonds, so it will competitively chemisorb more strongly and participate in the hydrogen bonding network, and so is going to be different from the other halides qualitatively and quantitatively. More work is needed here.

(vi) An alloy designed to better yield a low-energy hydrogen bonding network at the oxide surface could well be more stable in aqueous conditions, particularly in the presence of halides. It is suggestive that many of the existing protective oxide films will have such a network.

The analysis above focuses on the effect of chloride on local dissolution and breakdown, not the mean-field effects in terms of global corrosion rates. One important term for the latter is changes in the thermodynamic driver for dissolution, for instance terms due to aqueous MCl_x complexes such as the tetrachloroaluminate ion (e.g., references[64-65]) as mentioned earlier. In addition to thermodynamics, kinetics will matter and may be dominant. As a first approximation dissolution can be considered as time-reversed crystal growth, one can use the early formulation of Frank[108] as well as other work (e.g., references[108-114]); for an overview see Sangwal.[115] Some of the relevant mathematics such as the importance of the weighted mean curvature[116] as a measure of the chemical potential has been recently reviewed in the context of nanoparticle growth.[106]

If dissolution is considered as a statistical average of nucleation then growth of a three-dimensional nanoscale pits, the surface free energy comes directly into the problem—one has the conventional

heterogeneous nucleation and growth problem of a hemisphere or an inverse Winterbottom shape (see references in Marks and Peng[106]). The surface free energy does not explicitly come into the kinetics for layer-by-layer dissolution, but does indirectly if one assumes that the free energy of a surface step scales with the surface free energy of the parent flat surface. Nucleation now would involve a conventional two-dimensional nucleation and growth problem with the step energy per unit length. If the atomistic nucleation and growth is translated to a continuum approximation, one then has kinetic Wulff shapes. In all of the above the reduction of surface free energy with chloride chemisorption will, in a mean-field sense, increase the driver for corrosion (using the term Driver as defined earlier), although this statement should be treated with caution due to the large anisotropy with surface crystallography of the surface energy changes as discussed earlier, so mean-field models may be misleading.

Finally, it is worth stressing that protective oxide films are almost certainly not conformal, but will contain nanoscale grains with spatially varying crystallographic orientations and exposed surfaces, as well as galvanic potentials across the oxide. There will also be defects in the underlying alloy ranging from dislocations to grain boundaries and Kirkendall voids both in the metal and at the interface. While the idealized models herein can be used to extract key components of the physics, they do not describe the details of a real alloy in use where in all probability a range of processes are occurring all linked to different local Triggers, but with a common Driver.

ACKNOWLEDGMENTS

REFERENCES

1. P. Monnartz, *Metallurgie* 8 (1911): p. 161-176.
2. E. Devito, P. Marcus, *Surf. Interface Anal.* 19, 1-12 (1992): p. 403-408.
3. C.O.A. Olsson, *Corros. Sci.* 37, 3 (1995): p. 467-479.
4. R.F.A. Jargelius-Pettersson, *Corrosion* 54, 2 (1998): p. 162-168.
5. N.J.E. Dowling, Y.H. Kim, S.K. Ahn, Y.D. Lee, *Corrosion* 55, 2 (1999): p. 187-199.
6. L. Wegrelius, F. Falkenberg, I. Olefjord, *J. Electrochem. Soc.* 146, 4 (1999): p. 1397-1406.
7. A.C. Lloyd, J.J. Noel, N.S. McIntyre, D.W. Shoesmith, *JOM-US* 57, 1 (2005): p. 31-35.
8. J.R. Hayes, J.J. Gray, A.W. Szmodis, C.A. Orme, *Corrosion* 62, 6 (2006): p. 491-500.
9. M.J. Duarte, J. Klemm, S.O. Klemm, K.J. Mayrhofer, M. Stratmann, S. Borodin, A.H. Romero, M. Madinehei, D. Crespo, J. Serrano, S.S. Gerstl, P.P. Choi, D. Raabe, F.U. Renner, *Science* 341, 6144 (2013): p. 372-376.
10. D.D. Macdonald, *Pure Appl. Chem.* 71, 6 (1999): p. 951-978.
11. Z. Szklarska-Smialowska, *Corros. Sci.* 41, 9 (1999): p. 1743-1767.
12. P. Schmuki, *J. Solid State Electrochem.* 6, 3 (2002): p. 145-164.
13. C.O.A. Olsson, D. Landolt, *Electrochim. Acta* 48, 9 (2003): p. 1093-1104.
14. D.D. Macdonald, *Electrochim. Acta* 56, 4 (2011): p. 1761-1772.
15. V. Maurice, P. Marcus, *Electrochim. Acta* 84 (2012): p. 129-138.
16. P.M. Natishan, W.E. O'Grady, *J. Electrochem. Soc.* 161, 9 (2014): p. C421-C432.
17. J. Soltis, *Corros. Sci.* 90 (2015): p. 5-22.
18. D.J. Srolovitz, *Acta Metall. Mater.* 37, 2 (1989): p. 621-625.
19. B.J. Spencer, P.W. Voorhees, S.H. Davis, *Phys. Rev. Lett.* 67, 26 (1991): p. 3696-3699.
20. A.J. Pidduck, D.J. Robbins, A.G. Cullis, W.Y. Leong, A.M. Pitt, *Thin Solid Films* 222, 1-2 (1992): p. 78-84.
21. R.K. Bordia, A. Jagota, *J. Am. Ceram. Soc.* 76, 10 (1993): p. 2475-2485.
22. B.J. Spencer, S.H. Davis, P.W. Voorhees, *Phys. Rev. B* 47, 15 (1993): p. 9760-9777.
23. B.J. Spencer, P.W. Voorhees, S.H. Davis, *J. Appl. Phys.* 73, 10 (1993): p. 4955-4970.
24. W.H. Yang, D.J. Srolovitz, *Phys. Rev. Lett.* 71, 10 (1993): p. 1593-1596.
25. B.J. Spencer, D.I. Meiron, *Acta Metall. Mater.* 42, 11 (1994): p. 3629-3641.
26. L.B. Freund, *Int. J. Solids Struct.* 32, 6-7 (1995): p. 911-923.
27. J.E. Guyer, P.W. Voorhees, *Phys. Rev. Lett.* 74, 20 (1995): p. 4031-4034.
28. J.E. Guyer, P.W. Voorhees, *Phys. Rev. B* 54, 16 (1996): p. 11710-11724.
29. J. Tersoff, *Phys. Rev. Lett.* 77, 10 (1996): p. 2017-2020.
30. W. Barvosa-Carter, M.J. Aziz, L.J. Gray, T. Kaplan, *Phys. Rev. Lett.* 81, 7 (1998): p. 1445-1448.
31. H. Gao, W.D. Nix, *Annu. Rev. Mater. Sci.* 29, 1 (1999): p. 173-209.
32. J. Muller, M. Grant, *Phys. Rev. Lett.* 82, 8 (1999): p. 1736-1739.
33. B.J. Spencer, P.W. Voorhees, J. Tersoff, *Phys. Rev. B* 64, 23 (2001): p. 235318.
34. F.Q. Yang, *Electrochem. Solid State Lett.* 9, 2 (2006): p. C44-C47.
35. T.P. Hoar, *Corros. Sci.* 7, 6 (1967): p. 341-355.
36. N. Sato, *Electrochim. Acta* 16, 10 (1971): p. 1683-1692.
37. Y. Xu, M. Wang, H.W. Pickering, *J. Electrochem. Soc.* 140, 12 (1993): p. 3448-3457.
38. Y.Y. Tang, R. Ballarini, *J. Mech. Phys. Solids* 59, 2 (2011): p. 178-193.
39. A.H. Heuer, H. Kahn, P.M. Natishan, F.J. Martin, L.E. Cross, *Electrochim. Acta* 58 (2011): p. 157-160.
40. P. Zubko, G. Catalan, A.K. Tagantsev, *Annu. Rev. Mater. Res.* 43, 1 (2013): p. 387-421.
41. H.H. Strehblow, *Werkst. Korros./Mater. Corros.* 27, 11 (1976): p. 792-799.
42. H.H. Strehblow, B. Titze, *Corros. Sci.* 17, 6 (1977): p. 461-472.
43. H.H. Strehblow, *Werkst. Korros./Mater. Corros.* 35, 10 (1984): p. 437-448.
44. B. Macdougall, M. Cohen, *J. Electrochem. Soc.* 124, 8 (1977): p. 1185-1190.
45. W. Khalil, S. Haupt, H.H. Strehblow, *Werkst. Korros./Mater. Corros.* 36, 1 (1985): p. 16-21.
46. F. Di Quarto, *J. Electrochem. Soc.* 131, 12 (1984): p. 2901-2906.
47. S.P. Mattin, G.T. Burstein, *Phil. Mag. Lett.* 76, 5 (1997): p. 341-347.
48. S.Y. Yu, W.E. O'Grady, D.E. Ramaker, P.M. Natishan, *J. Electrochem. Soc.* 147, 8 (2000): p. 2952-2958.
49. T.P. Hoar, D.C. Mears, G.P. Rothwell, *Corros. Sci.* 5, 4 (1965): p. 279-289.
50. P. Marcus, V. Maurice, H.H. Strehblow, *Corros. Sci.* 50, 9 (2008): p. 2698-2704.
51. N. Pineau, C. Minot, V. Maurice, P. Marcus, *Electrochem. Solid State Lett.* 6, 11 (2003): p. B47-B51.
52. A. Bouzoubaa, B. Diawara, V. Maurice, C. Minot, P. Marcus, *Corros. Sci.* 51, 4 (2009): p. 941-948.
53. A. Bouzoubaa, D. Costa, B. Diawara, N. Audiffren, P. Marcus, *Corros. Sci.* 52, 8 (2010): p. 2643-2652.
54. L.F. Lin, C.Y. Chao, D.D. Macdonald, *J. Electrochem. Soc.* 128, 6 (1981): p. 1194-1198.
55. D.D. Macdonald, *J. Electrochem. Soc.* 139, 12 (1992): p. 3434-3449.
56. D.D. Macdonald, X.W. Lei, *J. Electrochem. Soc.* 163, 13 (2016): p. C738-C744.
57. E. Kirkendall, L. Thomassen, C. Uethegrove, *Trans. Am. Inst. Min. Metall. Eng.* 133 (1939): p. 186-203.

58. E.O. Kirkendall, *Trans. Am. Inst. Min. Metall. Eng.* 147 (1942): p. 104-109.
59. A.D. Smigelskas, E.O. Kirkendall, *Trans. Am. Inst. Min. Metall. Eng.* 171 (1947): p. 130-142.
60. L.C.C. Dasilva, R.F. Mehl, *Trans. Am. Inst. Min. Metall. Eng.* 191, 2 (1951): p. 155-173.
61. P.E. Doherty, R.S. Davis, *Ann. N.Y. Acad. Sci.* 101, 3 (1963): p. 787-790.
62. K.N. Tu, *Annu. Rev. Mater. Sci.* 15 (1985): p. 147-176.
63. H. Nakajima, *JOM-J. Miner. Metals Mater. Soc.* 49, 6 (1997): p. 15-19.
64. Y. Marcus, *Coord. Chem. Rev.* 2, 2 (1967): p. 195-238.
65. Y. Marcus, *Coord. Chem. Rev.* 2, 3 (1967): p. 257-297.
66. S.E. Traubenberg, R.T. Foley, *J. Electrochem. Soc.* 118, 7 (1971): p. 1066.
67. P.J. Eng, T.P. Trainor, G.E. Brown, G.A. Waychunas, M. Newville, S.R. Sutton, M.L. Rivers, *Science* 288, 5468 (2000): p. 1029-1033.
68. X.G. Wang, A. Chaka, M. Scheffler, *Phys. Rev. Lett.* 84, 16 (2000): p. 3650-3653.
69. M. Digne, P. Sautet, P. Raybaud, P. Euzen, H. Toulhoat, *J. Catal.* 211, 1 (2002): p. 1-5.
70. Z. Lodziana, J.K. Norskov, P. Stoltze, *J. Chem. Phys.* 118, 24 (2003): p. 11179-11188.
71. M. Digne, P. Sautet, P. Raybaud, P. Euzen, H. Toulhoat, *J. Catal.* 226, 1 (2004): p. 54-68.
72. A. Dyan, C. Azevedo, P. Cenedese, P. Dubot, *Appl. Surf. Sci.* 254, 13 (2008): p. 3819-3828.
73. J. Ciston, A. Subramanian, L.D. Marks, *Phys. Rev. B* 79, 8 (2009): p. 085421.
74. E. Carrasco, M.A. Brown, M. Sterrer, H.J. Freund, K. Kwapien, M. Sierka, J. Sauer, *J. Phys. Chem. C* 114, 42 (2010): p. 18207-18214.
75. J. Ciston, A. Subramanian, D.M. Kienzle, L.D. Marks, *Surf. Sci.* 604, 2 (2010): p. 155-164.
76. C. Ebensperger, B. Meyer, *Phys. Status Solidi B* 248, 10 (2011): p. 2229-2241.
77. B. Malki, O. Le Bacq, A. Pasturel, B. Baroux, *J. Electrochem. Soc.* 161, 10 (2014): p. C486-C493.
78. S.E. Mason, C.R. Iceman, T.P. Trainor, A.M. Chaka, *Phys. Rev. B* 81, 12 (2010): p. 125423.
79. S. Aboud, J. Wilcox, G.E. Brown, *Phys. Rev. B* 83, 12 (2011): p. 125407.
80. G. Rubasinghege, V.H. Grassian, *Chem. Commun.* 49, 30 (2013): p. 3071-3094.
81. P. Fenter, S.S. Lee, *MRS Bull.* 39, 12 (2014): p. 1056-1061.
82. J. Wirth, H. Kirsch, S. Wloszyk, Y.J. Tong, P. Saalfrank, R.K. Campen, *Phys. Chem. Chem. Phys.* 18, 22 (2016): p. 14822-14832.
83. W. Zhao, M. Bajdich, S. Carey, A. Vojvodic, J.K. Norskov, C.T. Campbell, *ACS Catal.* 6, 11 (2016): p. 7377-7384.
84. S. Alavi, D.C. Sorescu, D.L. Thompson, *J. Phys. Chem. B* 107, 1 (2003): p. 186-195.
85. Y. Li, Y.F. Zhang, L.M. Wu, Y.J. Xu, W.K. Chen, J.Q. Li, *Chem. Phys.* 328, 1-3 (2006): p. 236-242.
86. K.N. Nigussa, K.L. Nielsen, O. Borck, J.A. Stovneng, *Corros. Sci.* 53, 11 (2011): p. 3612-3622.
87. K.N. Nigussa, K.L. Nielsen, O. Borck, J.A. Stovneng, *Surf. Sci.* 653 (2016): p. 211-221.
88. M. Menetrey, A. Markovits, C. Minot, *Surf. Sci.* 566 (2004): p. 693-697.
89. A. Bouzoubaa, B. Diawara, V. Maurice, C. Minot, P. Marcus, *Corros. Sci.* 51, 9 (2009): p. 2174-2182.
90. X. Wei, C.F. Dong, Z.H. Chen, K. Xiao, X.G. Li, *Appl. Surf. Sci.* 355 (2015): p. 429-435.
91. P. Blaha, K. Schwarz, G. Madsen, D. Kvasnicka, J. Luitz, *Wien2k, an Augmented Plane Wave + Local Orbitals Program for Calculating Crystal Properties* (Vienna, Austria: Technische Universität Wien, 2001).
92. J.P. Perdew, K. Burke, M. Ernzerhof, *Phys. Rev. Lett.* 77, 18 (1996): p. 3865-3868.
93. W. Kahan, *Commun. ACM* 8, 1 (1965): p. 40.
94. L.D. Marks, *J. Chem. Theory Comput.* 9, 6 (2013): p. 2786-2800.
95. J. Sun, A. Ruzsinszky, J.P. Perdew, *Phys. Rev. Lett.* 115, 3 (2015): p. 036402.
96. H. Peng, Z.-H. Yang, J.P. Perdew, J. Sun, *Phys. Rev. X* 6, 4 (2016): p. 041005.
97. F. Tran, J. Stelzl, D. Koller, T. Ruh, P. Blaha, *Phys. Rev. B* 96, 5 (2017): p. 054103.
98. J.A. Enterkin, A.E. Becerra-Toledo, K.R. Poeppelmeier, L.D. Marks, *Surf. Sci.* 606, 3-4 (2012): p. 344-355.
99. L. Pauling, *J. Am. Chem. Soc.* 51, 1-4 (1929): p. 1010-1026.
100. R.F.W. Bader, *Chem. Rev.* 91, 5 (1991): p. 893-928.
101. I. Batyrev, A. Alavi, M.W. Finnis, *Faraday Discuss.* 114 (1999): p. 33-43.
102. K. Reuter, M. Scheffler, *Phys. Rev. B* 65, 3 (2002): p. 035406.
103. X.X. Yu, A. Gulec, A. Yoon, J.M. Zuo, P.W. Voorhees, L.D. Marks, *Nano Lett.* 17, 8 (2017): p. 4661-4664.
104. L.D. Marks, A.N. Chiaramonti, S.U. Rahman, M.R. Castell, *Phys. Rev. Lett.* 114, 22 (2015): p. 226101.
105. D. van der Spoel, P.J. van Maaren, P. Larsson, N. Timneanu, *J. Phys. Chem. B* 110, 9 (2006): p. 4393-4398.
106. L.D. Marks, L. Peng, *J. Phys. Condens. Matter* 28, 5 (2016): p. 053001.
107. N. Cabrera, N.F. Mott, *Rep. Prog. Phys.* 12 (1948): p. 163-184.
108. F.C. Frank, "On the Kinematic Theory of Crystal Growth and Dissolution Processes," in *Growth and Perfection of Crystals*, eds. R.H. Doremus, B.W. Roberts, D. Tumbull (New York, NY: Wiley, 1958).
109. J. Villain, *Nature* 350, 6316 (1991): p. 273-274.
110. R.F. Sekerka, *Cryst. Res. Technol.* 40, 4-5 (2005): p. 291-306.
111. J.E. Taylor, J.W. Cahn, C.A. Handwerker, *Acta Metall. Mater.* 40, 7 (1992): p. 1443-1474.
112. V. Gorshkov, A. Zavalov, V. Privman, *Langmuir* 25, 14 (2009): p. 7940-7953.
113. J.S. Wettlaufer, M. Jackson, M. Elbaum, *J. Phys. A Math. Gen.* 27 (1994): p. 5957-5967.
114. V. Jindal, F. Shahedipour-Sandvik, *J. Appl. Phys.* 106, 8 (2009): p. 083115.
115. K. Sangwal, *Etching of Crystals Theory, Experiment and Application*, vol. 15 (New York, NY: Elseview, 1987).
116. J.E. Taylor, *Acta Metall. Mater.* 40, 7 (1992): p. 1475-1485.
117. L.D. Marks, *Surf. Sci.* 604, 11-12 (2010): p. 878-881.
118. J. Nocedal, S. Wright, *Numerical Optimization* (New York, NY: Springer-Verlag New York, 2006).
119. O. Warschkow, M. Asta, N. Erdman, K.R. Poeppelmeier, D.E. Ellis, L.D. Marks, *Surf. Sci.* 573, 3 (2004): p. 446-456.
120. G. Makov, M.C. Payne, *Phys. Rev. B* 51, 7 (1995): p. 4014-4022.
121. J. Neugebauer, M. Scheffler, *Phys. Rev. B* 46, 24 (1992): p. 16067-16080.
122. J.P. Perdew, Y. Wang, *Phys. Rev. B* 45, 23 (1992): p. 13244-13249.
123. J. Tao, J.P. Perdew, V.N. Staroverov, G.E. Scuseria, *Phys. Rev. Lett.* 91, 14 (2003): p. 146401.
124. V.N. Staroverov, G.E. Scuseria, J.M. Tao, J.P. Perdew, *J. Chem. Phys.* 119, 23 (2003): p. 12129-12137.
125. R. Armiento, A.E. Mattsson, *Phys. Rev. B* 72, 8 (2005): p. 085108.
126. A.E. Mattsson, D.R. Jennison, *Surf. Sci.* 520, 1-2 (2002): p. L611-L618.
127. J.P. Perdew, A. Ruzsinszky, G.I. Csonka, O.A. Vydrov, G.E. Scuseria, L.A. Constantin, X. Zhou, K. Burke, *Phys. Rev. Lett.* 100, 13 (2008): p. 136406.
128. A.D. Becke, *J. Chem. Phys.* 98, 7 (1993): p. 5648-5652.
129. C. Adamo, V. Barone, *J. Chem. Phys.* 110, 13 (1999): p. 6158-6170.
130. J. Heyd, G.E. Scuseria, M. Ernzerhof, *J. Chem. Phys.* 118, 18 (2003): p. 8207-8215.
131. J. Heyd, G.E. Scuseria, M. Ernzerhof, *J. Chem. Phys.* 124, 21 (2006): p. 219906.
132. F. Tran, P. Blaha, *Phys. Rev. B* 83, 23 (2011): p. 235118.
133. S. Grimme, *J. Comput. Chem.* 27, 15 (2006): p. 1787-1799.
134. S. Grimme, J. Antony, S. Ehrlich, H. Krieg, *J. Chem. Phys.* 132, 15 (2010): p. 154104.
135. S. Grimme, S. Ehrlich, L. Goerigk, *J. Comput. Chem.* 32, 7 (2011): p. 1456-1465.
136. A.D. Boese, *ChemPhysChem* 16, 5 (2015): p. 978-985.
137. J. Sun, R.C. Remsing, Y. Zhang, Z. Sun, A. Ruzsinszky, H. Peng, Z. Yang, A. Paul, U. Waghmare, X. Wu, M.L. Klein, J.P. Perdew, *Nat. Chem.* 8, 9 (2016): p. 831-836.

APPENDIX

DFT Calculations of Oxide Surfaces

While DFT codes are often used as black-boxes, there are many traps, so a few general comments about DFT methods for oxide surfaces are provided here. DFT exploits a linearization of the many-body quantum

mechanical problem, which yields ground-state orbitals as eigensolutions that are different from the single-electron states, but in many cases are good approximations to them. Atomic positions tend to be quite accurate (once the lattice parameters are rescaled), energies reasonably accurate, and band gaps wrong. Because pure DFT is a linearization that produces orbitals different from the single electron wavefunctions, there is no a priori reason that the band gap should be correct, particularly as this is an excited-state property. Most available codes will find a local minimum of the enthalpy, which can be an issue. If the original starting point is inappropriate, the local minimum may be (often is) a "better" but still inappropriate configuration. It is therefore important to search an adequate space of initial starting points, although these details are rarely reported in publications and often converged atomic positions are not published.[117] For magnetic systems (i.e., when there is non-zero spin on some atoms) the space is larger, as different magnetic states may be local minima. Sometimes thin slabs (normal to the surface) are used with atomic positions fixed so they cannot move to model bulk. This is based upon a common misconception of what controls optimizations. It is known (see references in Marks[94] and also Nocedal and Wright[118]) that optimization depends upon the number and clustering of the eigenvectors, which for optimizing atomic positions are the elastic eigen-waves. Fixing atoms does not necessarily reduce the number of significant eigenvectors, and can introduce artifacts. It is better to check that the bond-valence sums (BVS) in the center of the slab are a good approximation to what they are in the bulk[98] (and/or other properties such as the density of states).

It is quite easy to calculate misleading energies if basic chemical principles are not followed, for instance have cations in inappropriate valence states, surfaces which are over-oxidized or exceedingly reduced. This can be avoided by using standard BVS methods, which are very important for oxide surfaces.[98] Non-bonded repulsions between oxygen atoms and, independently, cations also need to be considered carefully, as these can be very important.[119] With care reasonable approximations for configurations with unbalanced charges or dipoles (e.g., references[120-121]) can be calculated, although to avoid singularities in the energy some approximations are made. For a system with unbalanced dipolar fields, such as when there is band-bending across a metal/oxide/vacuum system during oxidation, one can add artificial terms to cancel the long-range dipole field. These technical issues are not relevant to any of the structures herein as they are all valence neutral, and the use of inversion symmetry means that from parity that there are no net dipoles.

There are inevitable compromises with the functional used. The earliest approach historically was the local density approximation (LDA; e.g., Perdew and Wang[122]). While this can give relatively good surface energies due to a fortuitous cancellation (e.g., references[122-124]), the other failings of the LDA are now well established. The most common functional currently used is the PBE generalized gradient approximation (GGA),[92] which, while it often gives very good results, can underestimate surface energies.[125-127] More recent functionals are better for surface energies because they more faithfully consider the long-range decay outside of the surface, most notable the PBEsol GGA,[127] but the gain has a cost. PBEsol is a softer functional, so it decreases the ionicity in oxides which is better represented using a PBE approach, albeit still underestimated compared to the higher-level orbital-DFT methods such as hybrids (e.g., references[128-132]) where fractional exact exchange terms are added. Unfortunately, hybrids are currently prohibitively computationally expensive for large unit cells. There are other new functionals which often improve results, although sometimes they do not; for instance a popular recent method adds a dispersion correct (e.g., references[133-135]), although it is not clear if this leads to improvements in hydrogen bonding energies.[136] Probably the best current approach is to simultaneously handle the long-range density decay outside of a surface using a metaGGA, for instance the recent SCAN functional[95,137] which can be supplemented with a dispersion correction.[96] Whether this is enough to also handle the reduced ionicity at oxide surfaces is not as yet completely clear as it is hard to find definitive experimental tests.

There are also trickier problems which are "buried" inside the numerical codes, and are often not apparent when they are used as black-box tools, for instance approximations in numerical differentiations, stability (conditioning) of integrations and differentiations, truncations of expansions, and the intrinsic limits of numerical accuracy even with modern double-precision coding. For instance, without techniques such as Kahan summations[93] it is easy to lose significant accuracy. Because quasi-Newton methods typically used to minimize the energy and also achieve self-consistency involve a numerical gradient simplex, the overall accuracy can degrade significantly, leading to a noisy optimization problem with local minima. This can lead to inaccuracies at the 1 meV to 10 meV level or larger unless care is taken to use "good" parameters which are not always well detailed in documentation and are part of the unwritten literature. With care, quite good agreement between experimental structures determined using methods such as x-ray or electron diffraction can be obtained, although rarely at what one would like for larger structures (100 to 1,000 atoms such as those herein) of experimental relevance, particularly if there is entropic disorder

(e.g., Marks, et al.[104]). Care is needed with the ab initio thermodynamics;[101-102] thermodynamics is never easy. Eventually what is called "chemical accuracy," corresponding to better than 1 kcal/mol will be achieved for large systems. Until then and in some cases beyond, in the author's opinion DFT calculations of oxide surfaces for corrosion are best considered as computational experiments which provide key information about the relevant Drivers (see *Background* section) because a real protective oxide has much more complexity at the nanoscale, elements of which are described in the *Discussion* section.